Effects of Non-Newtonian Viscosity and Suspended Particles on Torque Measurements in Rotational Viscometry

Lucas Volpi[1], Eric Cayeux[2], Rune W. Time[1] and Hans Joakim Skadsem[1,2]

[1]University of Stavanger, 4021 Stavanger, Norway
[2]Norwegian Research Centre, 4021 Stavanger, Norway

ABSTRACT

Accurate rheological characterization of fluids is of critical importance in a range of applications. A challenge associated with viscometric flows of non-Newtonian fluids is that both the shear rate and the shear stress will normally depend on the unknown viscosity of the fluid. A further complication arises when physical properties of the fluid, such as the spatial distribution of particles in particle-laden fluids, change over the course of the measurement. To gain insight into the flow of non-Newtonian fluids and particle suspensions in viscometric geometries, and how the fluid viscosity and neutrally buoyant particles affect the measurement, we solve the Navier-Stokes equation for a three-dimensional Couette geometry using the lattice Boltzmann method. With the model, secondary flows is observed at higher velocities, without major contributions in the torque measurement. When the particles are added, a large impact in the shear-rate field is noticed.

INTRODUCTION

Accurate characterization of the rheological properties is often necessary, and viscometers or more advanced rheometers are normally used for fluid characterization. In the particular case of the oil and gas industry, coaxial cylinder viscometers are the standard choice at the rig site.

Most often, conversions from raw measurements (angular velocities and torques) to shear rates and stresses are based on an assumption of a Newtonian fluid[1], for which the conversions are simple proportionality rules. However, for non-Newtonian fluids, these simple conversions are not sufficient to obtain a correct flow-curve[2] as the relations from rotational speed to wall shear rate, and from torque to wall shear stress depends on the unknown fluid viscosity. Secondary flows must be accounted for, whether or not end-effects take place depends not only on the rotation applied, but also on the rheological behaviour of the fluid. Time *et al*[3] explored experimentally the presence of end-effects in a rheometer-like geometry. With the aid of a dye, it was possible to notice that the secondary flows were present and that those could also form cusps that could change the boundary condition – which would directly impact the stress estimation.

In contrast with the Newtonian simplification, Skadsem and Saasen[4] recently analysed the effects of power-law and Newtonian assumptions on the wall shear rate for Herschel-Bulkley fluids in steady state laminar flows, with a particular emphasis on how the ratio between radii can affect the quality of the hypothesis in the estimation of parameters.

Numerical simulation present a flexible alternative to estimate the fluid dynamics. Lac and Parry[5] used computational fluid dynamic (CFD) software to model a concentric cylinder rheometer and to provide an inverse method for estimating the steady state rheological parameters of the fluid using the simulation data to extract the inverse model. In this case, the rheometer presented a rotating cylinder and a fixed bob, where the bob has a conical region at the top and a flat section at the bottom.

The lattice-Boltzmann method (LBM), even though computer-intensive, can adapt to both non-Newtonian behaviour and complex boundary conditions in unsteady flows. This last property makes the method well-suited for numerical simulation of problems with moving boundaries, for instance flows involving particle suspensions.

In this work, LBM is used to solve the dynamics of a power-law fluid in a concentric cylinder measurement geometry. In this case, there is a moving bob and a fixed cylinder. The bob presents a flat top with a conical bottom region, as in contrast to the one analysed by Lac and Parry[5]. In a first part, the full three-dimensional geometry of the immersed region of the equipment is considered in the presence of a particle-free liquid. In a second part, the rheometer geometry is reduced to a two-dimensional cross-section, and the flow of a fluid containing neutrally buoyant particles is analyzed. The main goals of this research are to: (i) evaluate the existence of end-effects in a concentric cylindrical rheometer, as well as understand how those can affect the overall measurement even with a small gap between the cup and the bob, and (ii) observe how neutrally buoyant particles can impact the fluid rheological behaviour and the possible implications the particles can have on rheological measurements.

MODEL AND METHODS

To model the dynamic flow of fluid in the rheometer, the LBM is used. This approach is intrinsically transient[6] and thus is well-suited for capturing unsteady end-effects.

The lattice-Boltzmann model consists in the discretization of the space, the velocity and the time domains of the Boltzmann equation, which generally yields:

$$\mathcal{F}_l(\boldsymbol{X} + \boldsymbol{c}_l\Delta t, t + \Delta t) = \mathcal{F}_l(\boldsymbol{X}, t) + \mathcal{C}_l(\mathcal{F}_l, \boldsymbol{X}, \boldsymbol{V}), \tag{1}$$

where $\mathcal{F}_l$ is the velocity density distribution function on the direction of the l^{th} velocity vector of the lattice ($\boldsymbol{c}_l$), $\boldsymbol{X}$ and $\boldsymbol{V}$ are the Eulerian description of space and velocity, respectively. The last term, $\mathcal{C}_l$, is the collision operator. The bulk properties of the fluid are recovered by the statistical moments of $\boldsymbol{\mathcal{F}}$: $\rho = \sum_l \mathcal{F}_l$ and $\rho\boldsymbol{V} = \sum_l \boldsymbol{c}_l\mathcal{F}_l$.

The following hypotheses made either concerns the model, or are intrinsic of the methods. The LBM solves the compressible form of the Navier-Stokes equation. In order to address this, small numerical Mach numbers must be chosen. The constitutive relations, however, are kept for an incompressible fluid.

It is also considered that the particles are perfectly spherical and that they present a different time-scale in relation to the flow, and thus different simulation times can be employed to solve the fully coupled system. While some overlap between particles is expected during collision, the impact-related parameters are chosen as to avoid large overlaps[7].

At this point, the development of the model is split into two cases: (i) a three dimensional model of the rheometer and (ii) a cross-section where the particulate phase is added.

3-DIMENSIONAL MODEL

The first model is based on an annular shear-flow where the inner cylinder rotates. The cross-section of the rheometer is presented in **Fig. 1a** with the assumed boundary conditions. The moving bob presents a conical region at the bottom and a flat top. **Figure 1b** presents the fixed bob/moving cylinder configuration from Lac and Parry[5], which is not explored this work

For the three-dimensional case, the 19-velocities set is used – each defined by an arrow and the zero-velocity vector –, in accordance to **Fig.2**, as it presents a balanced compromise between accuracy and efficiency[1]. Each lattice consists in a cubic element with an edge of ΔX.

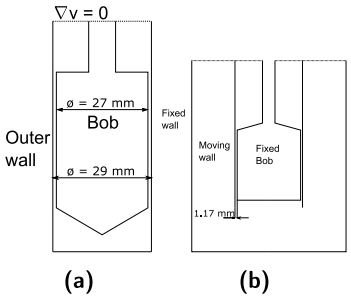

FIGURE 1: In (a) there is the moving bob/fixed cylinder configuration and in (b) the fixed bob/moving cylinder setup.

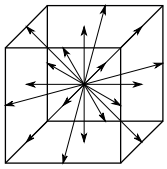

FIGURE 2: The D3Q19 lattice.

There are two boundary conditions in this case, a no slip wall condition, and a null velocity gradient at the interface between the liquid and the air. The former can be achieved by the use of the bounce-back method:

$$\mathcal{F}_l(\boldsymbol{X}, t+\Delta t) = \mathcal{F}_{\bar{l}}(\boldsymbol{X}_b, t) - 2w_l\rho\frac{\boldsymbol{c}_l \cdot \boldsymbol{V}_b}{c_s^2} \tag{2}$$

where $\bar{l}$ defines the opposite direction of l, i.e.: $\boldsymbol{c}_l = -\boldsymbol{c}_{\bar{l}}$, and $\boldsymbol{X}_b$ are the boundary nodes. The sub-index b specifies the boundary region, e.g.: $\boldsymbol{V}_b = \boldsymbol{V}(\boldsymbol{X}_b)$. The weight function w_l is dependent on the lattice type whereas the lattice sound velocity, c_s, is attached to both the numerical discretization and the lattice type.

The collision operator in this case is the Bhatnagar, Gross and Krook (BGK) operator, and is defined as:

$$\mathcal{C}_l^{bgk} = \frac{\Delta t}{\tau}(\mathcal{F}_l^{(eq)}(\rho, \boldsymbol{V}) - \mathcal{F}_l(\boldsymbol{X})), \tag{3}$$

where the relaxation time τ depends on the local viscosity $\eta = \rho c_s^2(\tau - 0.5\Delta t)$, and $\mathcal{F}_l^{(eq)}$ is the equilibrium distribution function approximated by $\mathcal{F}_l^{(eq)} = w_l\rho\big[1 + \frac{\boldsymbol{c}_l\cdot\boldsymbol{V}}{c_s^2} + \frac{(\boldsymbol{c}_l\cdot\boldsymbol{V})^2}{2c_s^4} - \frac{|\boldsymbol{V}|}{2c_s^2}\big]$.

For non-Newtonian fluids, the relaxation time is recalculated every time-step base on the local shear-rate[8], hereby estimated with the central difference scheme.

2-DIMENSIONAL SUSPENSION MODEL

This second model share most of the properties of the previous one. Due to the reduced dimension, the lattice only presents 9 velocities, one for each face of the lattice, other four connecting to the diagonals and the zero-velocity. In order to acknowledge the solid phase, the partially saturated method is adopted[9]. This changes the collision operator to:

$$\mathcal{C}_l = \left(1 - \sum \beta_p\right)\mathcal{C}_l^{bgk} + \left(\sum \beta_p\right)\mathcal{C}_l^s, \tag{4}$$

where β_p is a function of the volume fraction (b_p) of particle p in its respective lattice and is restricted by $\sum \beta_p \in [0, 1]$. The local volume fraction is estimated numerically by the *supersampling* method [10]. In this paper, the parameter[9] is simply $\beta_p = b_p$.

For the collision term, relaxing the fluid to the equilibrium distribution of solids for both incoming and bounced-back distributions provides a good accuracy [11]. This can be represented as [10,11]:

$$\mathcal{C}_l^s = [\mathcal{F}_{\bar{l}}(\boldsymbol{X}, t) - \mathcal{F}_{\bar{l}}^{(eq)}(\rho, \boldsymbol{V}_p)] - [\mathcal{F}_l(\boldsymbol{X}, t) - \mathcal{F}_l^{(eq)}(\rho, \boldsymbol{V}_p)], \tag{5}$$

where $\boldsymbol{V}_p = \boldsymbol{v}_p + \boldsymbol{\omega}_p \times (\boldsymbol{x}_p - \boldsymbol{X}_p)$ is the Eulerian description of a particle p with velocity $\boldsymbol{v}_p$, angular velocity $\boldsymbol{\omega}_p$ and centered at the point $\boldsymbol{x}_p$.

Each particle follows the discrete element method (DEM), where:

$$m\dot{\boldsymbol{v}} = \boldsymbol{f}_{p-p} + \boldsymbol{f}_w + \boldsymbol{f}_b + \boldsymbol{f}_f, \;\; I\dot{\boldsymbol{\omega}} = \boldsymbol{t}_{p-p} + \boldsymbol{t}_w + \boldsymbol{t}_b + \boldsymbol{t}_f, \tag{6}$$

where $\boldsymbol{f}_{p-p} = \sum_{i \neq j}^{N_p} \boldsymbol{f}_{ij}$, $\boldsymbol{f}_{ij}$ is the interaction force between particles p and n, and N_p is the total number of particles. Similarly, $\boldsymbol{t}_{p-p} = \sum_{i \neq j}^{N_p} \boldsymbol{t}_{ij}$ is the summation of the interaction torques, both in accordance to[12]:

$$\boldsymbol{f}_{ij} = \begin{cases} H(\delta_{ij})[k_n(\delta_{ij})\delta_{ij} + c_n \boldsymbol{v} \cdot \hat{\boldsymbol{e}}_n]\hat{\boldsymbol{e}}_n \\ H(\delta_{ij})[k_t(\delta_{ij})\delta_{ij} + c_t \boldsymbol{v} \cdot \hat{\boldsymbol{e}}_t]\hat{\boldsymbol{e}}_t \end{cases}, \;\; \boldsymbol{t}_{ij} = \boldsymbol{r}_i \times \boldsymbol{f}_{ij} \tag{7}$$

where $H(\delta_{ij})$ is the step function, and is 1 if there is overlap and 0 otherwise, and $\boldsymbol{r}_i = r_i \hat{\boldsymbol{e}}_n$ is the radial vector of particle i.

The generalized contact forces with the bob, $\boldsymbol{f}_b$ and $\boldsymbol{t}_b$, are treated similarly where the parameters k_n, k_t, c_n and c_t are adjusted to comport the difference in radii. The forces regarding the wall ($\boldsymbol{f}_w$ and $\boldsymbol{t}_w$) are a simplification of $\boldsymbol{f}_{p-p}$, where the wall radius is considered much larger then the particles' ($r_w \gg r_p$) and that a maximum overlap is expected for the calculation of the nonlinear stiffness and damping constants. This was estimated by the equilibrium in the scenario where it is simply supported by the surface: $m\boldsymbol{g} = \boldsymbol{f}_w(\delta_w)$. This strategy, in addition to the control of the stiffness[7], was chosen to minimize particle-particle/particle-bob overlaps within a feasible time-step.

Finally, the fluid forces are dependent on the solid collision operator[9]:

$$\boldsymbol{f}_f = \frac{\Delta\forall}{\Delta t} \sum_{\boldsymbol{X}_p} \beta(\boldsymbol{X}_p) \left[\sum_l \mathcal{C}_l^s \boldsymbol{c}_l\right], \;\; \boldsymbol{t}_f = \frac{\Delta\forall}{\Delta t} \sum_{\boldsymbol{X}_p} \beta(\boldsymbol{X}_p)(\boldsymbol{x}_p - \boldsymbol{X}_p) \times \left[\sum_l \mathcal{C}_l^s \boldsymbol{c}_l\right], \tag{8}$$

where $\Delta\forall = \Delta Z \Delta X^2$, and ΔZ is a numerical estimation of the particle's height in its respective lattice and the sub-index p refers to a particle-related variables.

RESULTS

In this section, the results for both models are presented. The non-Newtonian fluid followed a truncated power-law fit to $\eta(\dot{\gamma}) = 0.062|\dot{\gamma}|^{-0.404}$, chosen from available data from a rheometer of similar geometry. The torques on the bob were post-processed in accordance to $\boldsymbol{t}_b = \sum_{x_b}(\boldsymbol{x_b} - \boldsymbol{X_b}) \times (\boldsymbol{\tau} \cdot \boldsymbol{n})\Delta A(z)$,$\boldsymbol{n}$ is the vector orthonormal to the surface, and $\boldsymbol{\tau} = \eta(\dot{\gamma})\dot{\boldsymbol{\gamma}}$. The conical section was approximated by multiple cylinders with the same height as the lattice (ΔX).

Initially, the 3-dimensional model was solved. Each simulation was started with a stagnant fluid but the bob already at the desired rotating speed. The results presented are for instant $t = 6.5$ s, where steady-state estimation is made by the evaluating the relative variation of $\mathcal{F}_l$: $\xi = 1 - |\boldsymbol{\mathcal{F}}^{(t_i)}|/|\boldsymbol{\mathcal{F}}^{(t_f)}|$.

In **Fig. 3c**, three fields are presented for the rotational speed of $\Omega = 0.20$ rad/s: (a) the axial velocity, (b) the tangential velocity and (c) the shear-rate. The torque in the z-direction is calculated to be $t_{b_z} = 3.39$ μNm with a 3.4% percent contribution from the conical section and a 2.5% influence from the cylindrical section above the main cylinder.

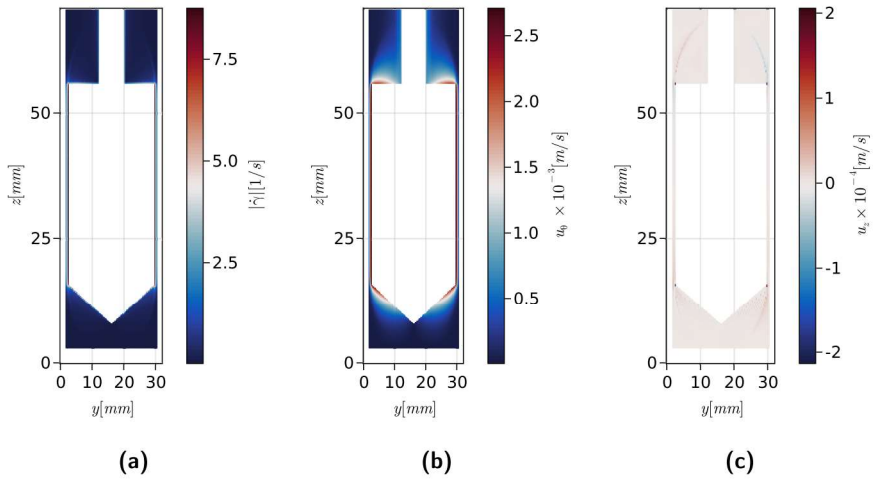

FIGURE 3: (a) Axial velocity, (b) tangential velocity and (c) strain-rate fields for the three-dimensional simulation with bob speed of $\omega = 0.2$ rad/s at $t = 6.5$ s.

The figure (**Fig. 4c**) is similarly organized and contains the results for the case $\Omega = 6.00$ rad/s. In this case, the components in the z-direction start to present a well-defined gradient in both the upper and lower sections of the rheometer.

For the second case, the estimated torque in the z-direction is $t_{b_z} = 38.93$ μNm, where approximately 5% originates from the conical region and close to 2.1% from the flat top of the bob.

For the flow of fluid with particles in suspension, the coupled LBM-DEM framework is solved asynchronously. A small uncertainty is added to both radial and angular intial positions to avoid an uniform perturbation in the fluid.

In **Fig. 6** the result at $t = 10.0$ s is presented for an angular velocity of $\Omega = 6.0$ rad/s at the bob. The particles are added in green over the velocity field for improved visualization. In this case, there were 50 particles, each with a radius of 0.1 mm.

In **Fig. 6a**, the red line represents the average radial position of the particles, along with black curves corresponding to the maximum and minimum limits. The dashed lines represent the radii of the bob and cup. The curve in **Fig. 6b** is the torque per length-unit

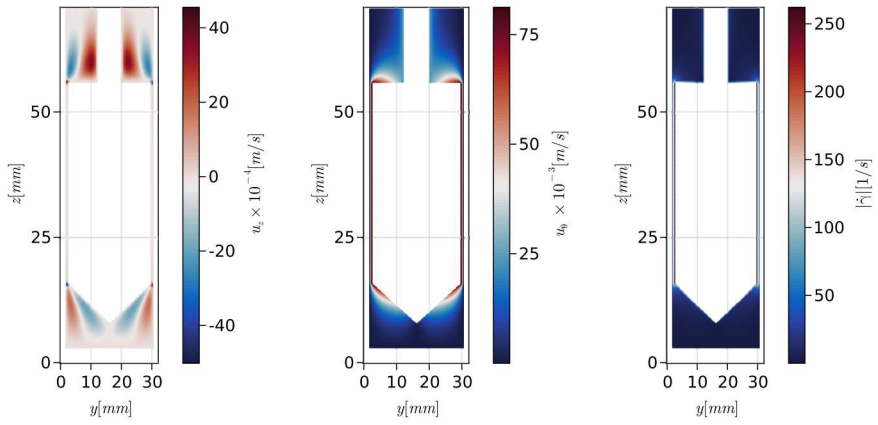

FIGURE 4: (a) Axial velocity, (b) tangential velocity and (c) strain-rate fields for the three-dimensional simulation with bob speed of $\omega = 6.0$ rad/s at $t = 6.5$ s.

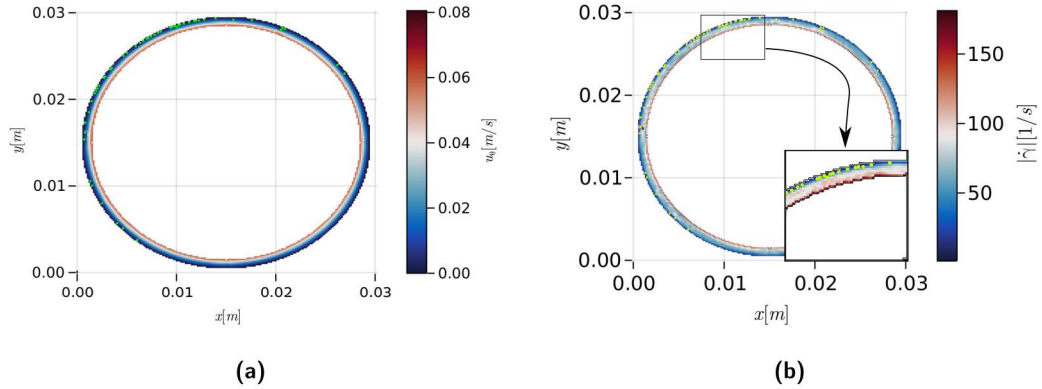

FIGURE 5: (a) total velocity, (b) strain-rate with bob speed of $\omega = 6.0$ rad/s at $t = 10.0$ s.

at the cross-section estimated by the momentum exchange method[6].

DISCUSSION

In the first case, with low rotational speed and using the three-dimensional geometry, the flow direction is predominantly tangential to the bob and, no relevant velocity field can be observed in the axial direction. When the speed is increased, the occurrence of end-effects is observed. In contrast, the shear-rate field seems to be unaffected.

When comparing the contributions in torque on each parts of the bob, a minor increase is observed, specially in the conical section (from 3.4% to 5%). Yet, the main torque contribution remains the one originating from the cylindrical section.

When particles are added, most of them agglomerate in small clusters. At some point, the impact between particles would disrupt an agglomerate. It is clear that after 10 s, the particles migrate to the low shear-rate region of the gap, as seen in **Fig. 6a**. Particles closer to the bob seem to disturb the shear-rate field, increasing it. This is a strong contrast with the expected behaviour of the Newtonian hypothesis, which might lead to an unrealistic simplification, particularly in small gaps. A correlation in the average

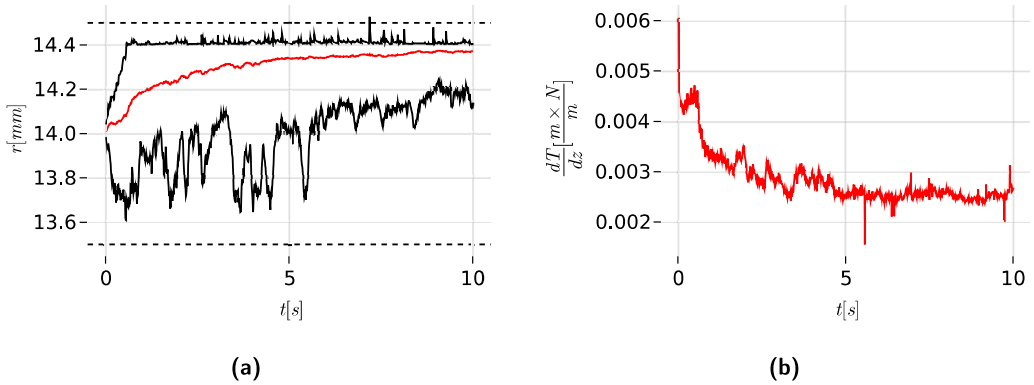

FIGURE 6: (a) Average radial displacement of particles through time. In red there is the mean value and the black lines define the maximum and minimum positions, and (b) the torque distribution at the cross-section, both with $\omega = 6.0$ rad/s at $t = 10.0$ s.

displacement and the torque per unit-length can observed when **Figs. 6a** and **6b** are analyzed. As the particles settle close to the low shear-rate region, the torque converges to a value larger than what is observed with the three-dimensional model.

Given the layers of numerical methods involved, some level of uncertainty is expected. The LBM with the BGK operator are generally second-order accurate schemes[6]. The partially saturated method is known to be accurate, specially for smaller lattice-size/particle ratios[13]. The bounce-back method used for the wall boundaries truncates the curvature into checkered sections, which adds to the uncertainties. The overlaps between particles and the walls, seen in **Fig. 6a**, might induce small errors in the continuity equation.

CONCLUDING REMARKS

In this paper the dynamic flow of a power-law fluid is analyzed for a concentric cylindrical rheometer with a rotating bob. A fully three-dimensional model has been studied for a particle-free fluid. Thereafter, a two-dimensional model of the flow of fluid containing neutrally-buoyant particles has been analyzed. The Navier-Stokes equation is solved with the LBM and, for the reduced case, is fully coupled with the DEM.

With these simulations, it is observed that at higher rotational speeds, secondary flows can be observed outside the main cylinder region. The presence of this secondary flow, however, does not seem to impact significantly the estimated shear-rate. This is a contrast with the observed in the moving cylinder/fixed bob configuration, where the secondary flow influences the measurement[5]. Finally, the contributions of both the flat and conical regions are slightly smaller then the standard correction factor[14] of 10% for similar geometry.

In the presence of particles, the shear-rate field become extremely particle-dependent, showing large variations close to clusters. There is also an increase in the measured torque which presented a correlation with the average particle position. This might imply that further corrections are necessary in the case of particle suspension.

The way forward is to propose a reduced order model that can be further used in the estimation of correction parameters and generalizing the model to other constitutive relations. As well as modelling the particle suspension in a 3D scale with non-neutrally buoyant particles.

REFERENCES

1. Kelessidis, V.C., Maglione, R., Bandelis, G. (2010). On the end-effect correcion for Couette type oil-field direct-indicating viscometers for Newtonian and non-Newtonian fluids. Journal of Petroleum Science and Engineering, **71**, 37-46.
2. Gücüyener H., Versan M. K. & Batmaz T. (2002) End Effect Evaluation in Rheological Measurement of Drilling Fluids Using Coutte Coaxial Cylinder Viscometer, Energy Sources, 24:5, 441-449, DOI: 10.1080/00908310252889942
3. Time, R. W., Rabenjafimanantsoa, H. A., Kelessidis, V. C., & Maglione, R. On End-Effect Correction for Couette Type Viscometers for Newtonian and Non-Newtonian Fluids.
4. Skadsem, H. J., Saasen, A. (2019). Concentric cylinder viscometer flows of Herschel-Bulkley fluids. Applied Rheology, **29**, 173-181. https://doi.org/10.1515/arh-2019-0015
5. Lac, E., Parry, A. (2010) Non-Newtonian End-Effects in Standard Oilfield Rheometers. Journal of Rheology **61**, 833.
6. Krüger, T., Kusumaatmaja, H., Kuzmin, A., et al. (2017). The lattice Boltzmann method. *Springer International Publishing*, **10(978-3)**, 4-15.
7. Norouzi, H. R., Zarghami, R., Sotudeh-Gharebagh, R., & Mostoufi, N. (2016). Coupled CFD-DEM modeling: formulation, implementation and application to multiphase flows. John Wiley & Sons.
8. Wang, C. H., & Ho, J. R. (2011). A lattice Boltzmann approach for the non-Newtonian effect in the blood flow. Computers & Mathematics with Applications, **62(1)**, 75-86.
9. Noble, D. R., & Torczynski, J. R. (1998). A lattice-Boltzmann method for partially saturated computational cells. International Journal of Modern Physics C, **9(08)**, 1189-1201.
10. Rettinger, C., & Rüde, U. (2017). A comparative study of fluid-particle coupling methods for fully resolved lattice Boltzmann simulations. Computers & Fluids, 154, 74-89.
11. Strack, O. E., & Cook, B. K. (2007). Three-dimensional immersed boundary conditions for moving solids in the lattice-Boltzmann method. International Journal for Numerical Methods in Fluids, 55(2), 103-125.
12. Tsuji, Y., Tanaka, T., & Ishida, T. (1992). Lagrangian numerical simulation of plug flow of cohesionless particle in a horizontal pipe. Powder Technology, 71, 239-250.
13. Han, Y., & Cundall, P. A. (2011). Resolution sensitivity of momentum-exchange and immersed boundary methods for solid–fluid interaction in the lattice Boltzmann method. International journal for numerical methods in fluids, 67(3), 314-327.
14. Mezger, T. G. (2006). The Rheology Handbook: For users of rotational and oscillatory rheometers. Vincentz network GmbH & Co. KG, Hannover, Germany.